A Geometric Variable-Strain Approach for Static Modeling of Soft Manipulators With Tendon and Fluidic Actuation

Federico Renda, Costanza Armanini, Vincent Lebastard, Fabien Candelier, and Frederic Boyer

***Abstract*—We propose a novel variable-strain parametrization for soft manipulators, which discretizes the continuous Cosserat rod model onto a finite set of strain basis functions. This approach generalizes the recently proposed piecewise-constant strain method to the case of non-constant strain sections. As for its predecessor, the discrete model is based on the relative pose between consecutive cross-sections and is provided in its minimal matrix form (Lagrangian-like). The novel variable-strain model is applied to the static equilibrium of tendon and/or fluidic actuated soft manipulators. It is shown that, for a specific choice of strain basis, exploiting the actuator geometry, the system is trivialized, providing useful tools for control and actuator routing design. Comparisons with the full continuous Cosserat model demonstrate the feasibility of the approach.**

***Index Terms*—Soft robotics, robot kinematics, robot control.**

I. Introduction

ONE of the main challenges of the soft robotics field is the development of mathematical models capable of describing the complex deformed configurations with both accuracy and simplicity [1]. Despite the great number of proposed solutions, many of the desired objectives are yet to be accomplished, especially for what concerns the applicability of the proposed methods in a control design prospective [2].

A. Brief State-of-the-Art (SoA) Modeling for Control

Lumped-mass models can be useful for soft robot simulation [3], [4], while they provide limited applicability to control desig due to the large number of Degrees of Freedom (DOFs) and the cumbersome relation between the continuous, distributed actuation and the robot configuration. Similar limitations are observed for Finite Element Method (FEM) based models [5]. Being based on continuum mechanics, FEM can accurately describe the action of the distributed actuation on the robot as well as its deformation under external and contact loads. However, they require sophisticated reduction tecniques in order to be employed as control design tools [6], [7]. Cosserat rod model has demonstrated excellent performance for what concerns the dynamic simulation of rod-like soft robots [8], [9], both in its planar [10], [11] and three dimensional [12], [13] formulations. The application of this method for control purposes relies on the implementation of fast numerical algorithms able to approximate the solution of the inverse [14] or the forward model [15], requiring ideally accurate sensory feedbacks in a real-life scenario. Furthermore, most soft robots are kinematically constrained multi-body systems composed of rigid as well as soft elements. In these cases, Cosserat approaches based on a displacement parametrization would result in stiff Differential-Algebraic-Equations (DAEs), which are difficult to be used for control purposes. This is especially true within the robotics community, where control designs are usually based on the minimal Lagrangian model of the system. Cosserat rod simulators have also been used for neural-network-based control in [16], [17] with the inherent limitations of any machine learning control design, such as poor generalization capability and high demand of data.

The widely popular constant-curvature models [18], [19] manage to describe the configuration of the robot with a fewer number of DOFs and have been succesfully used for modeling and control of soft robots [20]. However, these models require an extensive identification procedure since they are not based on the continuum mechanics of the robot arm and are applicable only when certain, strict conditions are satisfied. On the other end, in constrast to the above mentioned methods, the classical Lagrangian model of rigid-body robots represents a very useful and versatile tool for the control design of traditional robots [21]. In order to exploit this rich set of control tools developed for rigid robots, including flexible joint ones [22], some authors have developed serial-links Lagrangian models for soft robots that are suitable for control purposes due to their relative parametrization of the soft robotic arm [23]. However, as for the constant curvature models, these models require a case-by-case parameters identification in addition to be valid only under specific, limited conditions.

B. Constant-Strain Vs Variable-Strain Approach

In an effort to develop dynamics models based on the continuum mechanics of the robot arm and parametrized by a small set

Manuscript received October 15, 2019; accepted March 26, 2020. Date of publication April 6, 2020; date of current version April 24, 2020. This letter was recommended for publication by Associate Editor Prof. Girish Krishnan and Editor Cecilia Laschi upon evaluation of the reviewers' comments. This work was supported in part by the Khalifa University of Science and Technology under Award FSU-2018-08, RC1-2018-KUCARS and in part by ADEK Award for Research Excellence (AARE-2018-105). *(Corresponding author: Federico Renda.)*

Federico Renda is with the Khalifa University Center for Autonomous Robotic Systems and the Healthcare Engineering Innovation Center, Khalifa University of Science and Technology, Abu Dhabi 127788, UAE (e-mail: federico.renda@ku.ac.ae).

Costanza Armanini is with the Department of Mechanical Engineering, Khalifa University of Science and Technology, Abu Dhabi 127788, UAE (e-mail: costanza.armanini@ku.ac.ae).

Vincent Lebastard and Frederic Boyer are with the LS2N lab, Institut Mines Telecom Atlantique, 44307 Nantes, France (e-mail: vincent.lebastard@imt-atlantique.fr; frederic.boyer@imt-atlantique.fr).

Fabien Candelier is with the IUSTI lab, Aix-Marseille University (AMU), 13007 Marseille, France (e-mail: fabien.candelier@univ-amu.fr).

Digital Object Identifier 10.1109/LRA.2020.2985620

of relative, serial-link DOFs, more suitable for control purposes, the authors have developed a strain-based Cosserat approach called Piecewise-Constant-Strain (PCS) [24]. This approach extends the constant-curvature assumption to more general rod kinematics while providing a dynamic model in the standard minimal set of ordinary differential equations in the usual matrix form of traditional robotics. More recently, the PCS model has also been extended to hybrid soft-rigid multi-body systems including lumped, possibly flexible, DOFs [25]. In this letter, the PCS approach is generalized to the case of non-constant strains and applied to the static equilibrium of soft manipulators internally actuated by tendon and/or fluidic chambers with general routing (path taken by the actuator inside the arm). In this way, a simple discrete model is produced, particularly suitable for control purposes. During the process, a variable-strain geometric Jacobian for soft robotics is presented and a new generalized actuation matrix is proposed for the first time. With respect to the Constant-strain method, the Variable-strain approach allows the employment of any basis functions in the discretization process, instead of being limited to constant functions only. This may lead to a further reduction of the number of DOFs required to describe the system, with increased accuracy. Furthermore, specific basis functions can be selected to match design-specific parameters such as cross-section geometry and actuation routing. This highlights the relationship between these parameters and the robot arm deformation, facilitating the mechanical design.

C. Brief Comparison With Computational Mechanics SoA

Computational dynamics of Cosserat rods have been extensively developed after the pioneering works by J.C. Simo through the Geometrically-Exact Finite Elements Method (GEFEM) [26]–[28] to name a few. Similarly to the original work by Simo, most of these approaches are based on the parametrization of the beam configurations with fields of absolute transformations in the Lie Group SO(3) [26], its fibration S2xSO(2) [27] or SE(3) [28], [29]. In [30], the GEFEM has been reformulated with a strain-based interpolation. As shown by his authors, this alternative approach provides all the results of the standard transformation based parametrization, while offering further advantages in terms of accuracy, stability and robustness. In the presented letter, we exploit a similar idea but, instead of applying the usual FEM interpolations, we employ a Galerkin-Ritz approach where the strain fields are directly reduced on a functional basis defined over the entire rod. Moreover, the strain-based method is here more directly oriented towards robotics purposes, such as the derivation of the geometric Jacobian and a minimal (Lagrangian-like) matrix form especially useful for robot control applications. In this respect, the PCS approach, of which the present work proposes an extension, has been shown to encompass the geometric theory of robotics described in [31], which is realized by considering a rigid joint as an immaterial flexible beam with length one, constant strain and appropriate internal kinematics.

D. Contributions and Benefits of the Variable-Strain Approach

In this work, we focus on the static modeling of soft manipulators with tendon and fluidic actuation, an important and predominant formulation in the soft robotics community. In particular, we will show how, thanks to the proposed variable-strain method, a clever choice of the strain basis is able to transform the general non-linear, high dimensional static problem of FE/FD Cosserat formulations into a low dimensional, trivial form without any loss of information (and accuracy):

$$\boldsymbol{K}(\boldsymbol{q})\boldsymbol{q} = \boldsymbol{B}(\boldsymbol{q})\boldsymbol{\tau} \rightarrow \boldsymbol{q} = \boldsymbol{\tau}.$$

This is possible thanks to the reconstruction equations that take charge of all the nonlinearity of the system. The expression above is a very concise and effective representation of the active DOFs that, in a control perspective, shall rule the desired configuration and reject spurious deformations due to the passive DOFs.

II. Continuous Model

In this section, we present the continuous model of a Cosserat rod internally actuated by distributed tendons and/or fluidic chambers. A procedure similar to [24] is followed, with some additions that will be useful for the development of the new model (in particular Section II-B and part of Section II-C, II-D). As mentioned in the introduction, only the static equilibrium between the actuation load and the internal elasticity is considered.

A. Kinematics

A Cosserat rod is a continuous stack of rigid cross-sections parametrized by a material curvilinear abscissa $X \in [0, L]$ where L is the total length of the rod. Identifying each rigid cross-section with the moving frame rigidly attached to it, the configuration space of the rod is completely defined by a curve $\boldsymbol{g}(\cdot) : X \mapsto \boldsymbol{g}(X) \in SE(3)$ represented by the homogeneous matrix:

$$\boldsymbol{g} = \begin{pmatrix} \mathbf{R} & \mathbf{r} \\ \mathbf{0}^T & 1 \end{pmatrix}, \tag{1}$$

where $\mathbf{r}(X) \in \mathbb{R}^3$ is the position vector of the origin of the moving frame and $\mathbf{R}(X) \in SO(3)$ is the rotation matrix representing its orientation with respect to the spatial frame.

Considering the Lie algebra $\mathfrak{se}(3)$ of $SE(3)$, the derivative of $\boldsymbol{g}$ with respect to X can be written as:

$$\boldsymbol{g}' = \boldsymbol{g}\widehat{\boldsymbol{\xi}}\,, \tag{2}$$

where $\widehat{\boldsymbol{\xi}}(\cdot) : X \mapsto \widehat{\boldsymbol{\xi}}(X) \in \mathfrak{se}(3)$ defines the strain state of the rod (when compared with the reference configuration $\widehat{\boldsymbol{\xi}}^*$) and is given by:

$$\widehat{\boldsymbol{\xi}} = \begin{pmatrix} \tilde{\mathsf{k}} & \mathsf{u} \\ \mathbf{0}^T & 0 \end{pmatrix} \in \mathfrak{se}(3)\,,\ \boldsymbol{\xi} = \left(\mathsf{k}^T, \mathsf{u}^T\right)^T \in \mathbb{R}^6\,,$$

where $\mathsf{u}(X) \in \mathbb{R}^3$ represents the linear strains, $\mathsf{k}(X) \in \mathbb{R}^3$ the angular strains and $\tilde{}$ indicates the isomorphism between $\mathbb{R}^3$ and the algebra of skew symmetric matrices $\mathfrak{so}(3)$.

Then, the equality of mixed partial derivatives of $\boldsymbol{g}$ with respect to space X and time t yields:

$$\frac{\partial}{\partial t}\boldsymbol{g}' = \frac{\partial}{\partial X}\dot{\boldsymbol{g}} \Rightarrow \boldsymbol{\eta}' = \dot{\boldsymbol{\xi}} - \mathrm{ad}_{\boldsymbol{\xi}}\boldsymbol{\eta}\,, \tag{3}$$

where ad is the adjoint map defined in Appendix A and $\widehat{\boldsymbol{\eta}}(\cdot) : X \mapsto \widehat{\boldsymbol{\eta}}(X) \in \mathfrak{se}(3)$, defines the velocity of the moving frame and is given by:

$$\widehat{\boldsymbol{\eta}} = \boldsymbol{g}^{-1}\dot{\boldsymbol{g}} = \begin{pmatrix} \tilde{\mathsf{w}} & \mathsf{v} \\ \mathbf{0}^T & 0 \end{pmatrix} \in \mathfrak{se}(3)\,,\ \boldsymbol{\eta} = \left(\mathsf{w}^T, \mathsf{v}^T\right)^T \in \mathbb{R}^6\,,$$

where $\mathsf{v}(X) \in \mathbb{R}^3$ and $\mathsf{w}(X) \in \mathbb{R}^3$ are respectively the linear and angular velocity.

B. Integration of Kinematic Equations

Equation (2) is in the form $\boldsymbol{Y}' = \boldsymbol{Y}\boldsymbol{A}(X)$, and, following the approach of Magnus, it can be explicitly solved by a matrix function of the form $\boldsymbol{Y}(X) = \boldsymbol{Y}(0)\exp(\boldsymbol{\Omega}(X))$, where $\boldsymbol{\Omega}(X)$ is the so-called Magnus expansion of $\boldsymbol{A}(X)$ [32]. In the case of a soft manipulator, we have $\boldsymbol{g}(0) = \boldsymbol{I}_4$, the Magnus expansion of $\widehat{\boldsymbol{\xi}}(X)$ gives $\widehat{\boldsymbol{\Omega}}(X)$, an element of the Lie algebra $\mathfrak{se}(3)$, and the exponential exp is the exponential map in $SE(3)$ given in Appendix B [33]:

$$\boldsymbol{g}(X) = \exp\left(\widehat{\boldsymbol{\Omega}}(X)\right) . \tag{4}$$

Notice that, in the case of constant strain $\boldsymbol{\xi}(X) = \boldsymbol{\xi}$, the Lie brackets of $\widehat{\boldsymbol{\xi}}$ with its integral is null, *i.e.,* $[\int_0^X \widehat{\boldsymbol{\xi}} ds, \widehat{\boldsymbol{\xi}}] = 0$. Thus, we obtain $\widehat{\boldsymbol{\Omega}}(X) = \int_0^X \widehat{\boldsymbol{\xi}} ds = X\widehat{\boldsymbol{\xi}}$ that recovers the constant strain case [34]. For all the other non-commutative cases, the domain $[0, L]$ has to be discretized in intervals h, the Magnus expansion has to be truncated and the integrals therein have to be approximated by numerical quadrature [32]. In this work, we use the fourth order Zanna collocation approach with two-stage Gauss quadrature [35], which leads to:

$$\boldsymbol{g}(X+h) = \boldsymbol{g}(X)\exp\left(\frac{h\left(\widehat{\boldsymbol{\xi}}_1 + \widehat{\boldsymbol{\xi}}_2\right)}{2} + \frac{\sqrt{3}h^2\left[\widehat{\boldsymbol{\xi}}_1 + \widehat{\boldsymbol{\xi}}_2\right]}{12}\right) , \tag{5}$$

where $\widehat{\boldsymbol{\xi}}_1 = \widehat{\boldsymbol{\xi}}(X + h/2 - \sqrt{3}h/6)$ and $\widehat{\boldsymbol{\xi}}_2 = \widehat{\boldsymbol{\xi}}(X + h/2 + \sqrt{3}h/6)$.

Regarding the differential kinematic equation (3), by virtue of the identity $\mathrm{Ad}'_{\boldsymbol{g}^{-1}} = -\mathrm{ad}_{\boldsymbol{\xi}}\mathrm{Ad}_{\boldsymbol{g}^{-1}}$ and the Leibniz rule for the derivative of a product, it can be verified that the analytic solution of (3) is given by:

$$\boldsymbol{\eta}(X) = \mathrm{Ad}_{\boldsymbol{g}^{-1}} \int_0^X \mathrm{Ad}_{\boldsymbol{g}}\dot{\boldsymbol{\xi}} ds , \tag{6}$$

which also satisfy the initial condition $\boldsymbol{\eta}(0) = \mathbf{0}$. The operator Ad is the Adjoint map in $SE(3)$ defined in Appendix A.

C. Statics

We consider now the static equilibrium of a Cosserat rod internally actuated by a distributed tendons and/or fluidic chambers. To do that, let's consider a finite piece of rod virtually cut between two arbitrary point $X = a$ and $X = b$ as shown in Fig. 1. Neglecting the external loads, the forces acting on this finite piece are given by the internal forces exerted on a and b by the material with $X > b$ and $X < a$ respectively. It is important to notice that this material includes the internal tendon or fluidic chamber.

The internal elastic load exerted by the material with $X \in (X, L]$ is defined by:

$$\boldsymbol{\mathcal{F}}_i(\cdot) : X \mapsto \boldsymbol{\mathcal{F}}_i(X) = \left(\mathsf{M}_i^T(X), \mathsf{N}_i^T(X)\right)^T \in \mathbb{R}^6 ,$$

where $\mathsf{N}_i(X) \in \mathbb{R}^3$ and $\mathsf{M}_i(X) \in \mathbb{R}^3$ are respectively the internal elastic force and moment. Similarly, the internal actuation load exerted by the piece of tendon/chamber with $X \in [0, X)$ can be defined as:

$$\boldsymbol{\mathcal{F}}_a(\cdot) : X \mapsto \boldsymbol{\mathcal{F}}_a(X) = \left(\mathsf{M}_a^T(X), \mathsf{N}_a^T(X)\right)^T \in \mathbb{R}^6 ,$$

where $\mathsf{N}_a(X) \in \mathbb{R}^3$ and $\mathsf{M}_a(X) \in \mathbb{R}^3$ are respectively the actuation force and moment. Both $\boldsymbol{\mathcal{F}}_i$ and $\boldsymbol{\mathcal{F}}_a$ are defined in the local frame.

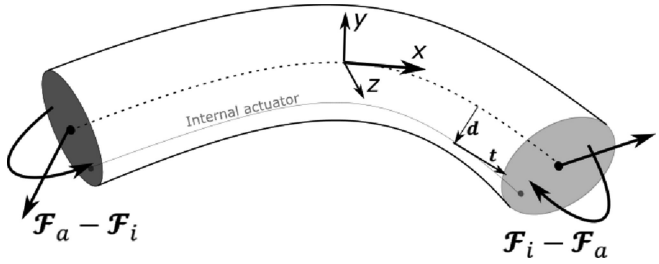

Fig. 1. Schematics of the static equilibrium of a finite piece of internally actuated Cosserat rod. $\boldsymbol{d}(X)$ represents the distance from the mid-line to the internal actuator and $\boldsymbol{t}(X)$ is the unit vector tangent to the actuator path.

The equilibrium of the finite piece $[a, b]$ with respect to the spatial frame is then given by:

$$\mathrm{Ad}^*_{\boldsymbol{g}(a)}\left(\boldsymbol{\mathcal{F}}_a(a) - \boldsymbol{\mathcal{F}}_i(a)\right) + \mathrm{Ad}^*_{\boldsymbol{g}(b)}\left(\boldsymbol{\mathcal{F}}_i(b) - \boldsymbol{\mathcal{F}}_a(b)\right) = \mathbf{0} , \tag{7}$$

where Ad^* is the co-Adjoint map in $SE(3)$ defined in Appendix A. Taking the limit of (7) for the interval $[a, b]$ going to 0 and using the identity $\mathrm{Ad}^{*\prime}_{\boldsymbol{g}} = \mathrm{Ad}^*_{\boldsymbol{g}}\mathrm{ad}^*_{\boldsymbol{\xi}}$ yields to the static ordinary differential equation and its final value [36].

$$\begin{aligned} &\left(\boldsymbol{\mathcal{F}}_i - \boldsymbol{\mathcal{F}}_a\right)' + \mathrm{ad}^*_{\boldsymbol{\xi}}\left(\boldsymbol{\mathcal{F}}_i - \boldsymbol{\mathcal{F}}_a\right) = \mathbf{0} , \\ &\boldsymbol{\mathcal{F}}_i(L) = \boldsymbol{\mathcal{F}}_a(L) , \end{aligned} \tag{8}$$

where ad^* is the co-adjoint map in $SE(3)$ defined in Appendix A.

D. Elasticity and Actuation Models

In order to complete the static equilibrium (8) a model for the internal elastic and the actuation loads has to be developed. For what concern the internal elastic load, one can take the derivative of any elastic energy potential $\Psi(\boldsymbol{\xi}) \in \mathbb{R}$ that better describes the rod elasticity. In practice, a Hook-like linear elastic law is normally used, which reads:

$$\boldsymbol{\mathcal{F}}_i(X) = \boldsymbol{\Sigma}(X)\left(\boldsymbol{\xi}(X) - \boldsymbol{\xi}^*\right) , \tag{9}$$

where $\boldsymbol{\Sigma}(X) \in \mathbb{R}^{6\times 6}$ is the elasticity tensor matrix, equal to $\boldsymbol{\Sigma} = diag(GJ_x, EJ_y, EJ_z, EA, GA, GA)$, E being the Young modulus, G the shear modulus, $A(X)$ the cross-sectional area and $J_x(X)$, $J_y(X)$, $J_z(X)$ the second moment of area of the cross-section around the $x-$, $y-$ and $z-$axis respectively (defined in Fig. 1).

With regards to the actuation load, it is obtained by computing the force and moment exerted by the internal tendon or chamber on the mid-line of the rod [37]. This is given by:

$$\boldsymbol{\mathcal{F}}_a(X) = \begin{bmatrix} \tilde{\boldsymbol{d}}(X)\boldsymbol{t}(X) \\ \boldsymbol{t}(X) \end{bmatrix} \tau , \tag{10}$$

where $\boldsymbol{d}(X) \in \mathbb{R}^3$ represents the distance from the mid-line to the internal actuator, $\boldsymbol{t}(X) \in \mathbb{R}^3$ is the unit vector tangent to the actuator path (see Fig. 1), and $\tau \in \mathbb{R}$ is the magnitude of the actuation force given by the tension of the tendon or by fluid

pressure for a fluidic actuation. Therefore, in the former τ takes a negative value while in the latter it becomes positive.

While the distance $\boldsymbol{d}(X)$ is fixed once for all by design, the tangent vector $\boldsymbol{t}(X)$ depends, in general, on the deformation $\boldsymbol{\xi}(X)$ of the soft manipulator [12], [13]. Going further into details, the unit tangent vector $\boldsymbol{t}(X)$ can be obtained by spatial differentiation of the position vector of the actuator, thus:

$$\boldsymbol{t}(X) = \frac{\boldsymbol{t}_c(X)}{\|\boldsymbol{t}_c(X)\|} = \frac{\left[\boldsymbol{g}^{-1}\left(\boldsymbol{g}\boldsymbol{d}\right)'\right]_3}{\|\boldsymbol{g}^{-1}\left(\boldsymbol{g}\boldsymbol{d}\right)'\|} = \frac{\left[\widehat{\boldsymbol{\xi}}\boldsymbol{d}(X) + \boldsymbol{d}'(X)\right]_3}{\|\widehat{\boldsymbol{\xi}}\boldsymbol{d}(X) + \boldsymbol{d}'(X)\|} , \tag{11}$$

where $\boldsymbol{d}(X)$ is expressed in homogeneous coordinates, $[\cdot]_3$ extracts the first three rows of a homogeneous vector and $\|\cdot\|$ takes the Euclidean norm.

E. Solution Continuum Model

Once supplemented with the elasticity (9) and actuation (10) equations, the continuous model (8) takes the form of a final value problem that can be converted into a initial value problem and solved for $\boldsymbol{\xi}(X)$. In order to accurately compare the variable-strain approach with its continuous counterpart, the explicit Ordinary Differential Equations (ODEs) of the continuous model are reported below.

$$\boldsymbol{\xi}' = \left(\boldsymbol{\Sigma} - \boldsymbol{A}\right)^{-1}\left(\boldsymbol{a} - \boldsymbol{b} - \boldsymbol{c}\right) , \tag{12}$$

where

$$\begin{aligned}
\boldsymbol{A} &= \sum_{i=1}^{n_a} \begin{bmatrix} \tilde{\boldsymbol{d}}_i \tilde{\boldsymbol{t}}_{ci}^2 \tilde{\boldsymbol{d}}_i & -\tilde{\boldsymbol{d}}_i \tilde{\boldsymbol{t}}_{ci}^2 \\ \tilde{\boldsymbol{t}}_{ci}^2 \tilde{\boldsymbol{d}}_i & -\tilde{\boldsymbol{t}}_{ci}^2 \end{bmatrix} \frac{\tau_i}{\|\boldsymbol{t}_{ci}\|^3} , \\
\boldsymbol{a} &= \sum_{i=1}^{n_a} \begin{bmatrix} \tilde{\boldsymbol{d}}_i' \boldsymbol{t}_{ci} \|\boldsymbol{t}_{ci}\|^2 - \tilde{\boldsymbol{d}}_i \tilde{\boldsymbol{t}}_{ci}^2 \left(\tilde{\mathsf{k}}\boldsymbol{d}_i' + \boldsymbol{d}_i''\right) \\ -\tilde{\boldsymbol{t}}_{ci}^2 \left(\tilde{\mathsf{k}}\boldsymbol{d}_i' + \boldsymbol{d}_i''\right) \end{bmatrix} \frac{\tau_i}{\|\boldsymbol{t}_{ci}\|^3} , \\
\boldsymbol{b} &= \mathrm{ad}^*_{\boldsymbol{\xi}} \left(\boldsymbol{\mathcal{F}}_i - \sum_{i=1}^{n_a} \boldsymbol{\mathcal{F}}_{ai} \right) , \\
\boldsymbol{c} &= \boldsymbol{\Sigma}'\left(\boldsymbol{\xi} - \boldsymbol{\xi}^*\right) - \boldsymbol{\Sigma}\boldsymbol{\xi}^{*'}
\end{aligned} \tag{13}$$

and n_a indicates the number of actuators. For more details, the reader can refer to [12], [36], [13].

III. Discrete Variable-Strain Model

In this section a new parametrization of the strain field $\boldsymbol{\xi}$ is proposed that yields to the definition of the variable-strain geometric Jacobian for soft manipulators, which, in turn, allows to project the static ODEs (8) and get a static algebraic equation in the new parametrization. The procedure followed is similar to the constant-strain case [34]. Explicit comparison is made along the way to highlight the novelty of the variable-strain approach.

A. Discrete Kinematics

The infinite dimensional strain field $\boldsymbol{\xi}$ can be discretized by selecting a set of vector functions to form a finite basis for the field. This can be represented as:

$$\boldsymbol{\xi}(X) = \boldsymbol{B}_q(X)\boldsymbol{q} + \boldsymbol{\xi}^* , \tag{14}$$

where $\boldsymbol{B}_q(X) \in \mathbb{R}^{6\times n}$ is a matrix function whose columns form the basis for the strain field $\boldsymbol{\xi}$ and $\boldsymbol{q} \in \mathbb{R}^n$ is the vector of coordinates in that basis, n being the number of degrees of freedom.

Inserting the finite dimensional strain (14) into the differential kinematic equation (6), yields to:

$$\boldsymbol{\eta}(X) = \left[\mathrm{Ad}_{\boldsymbol{g}}^{-1} \int_0^X \mathrm{Ad}_{\boldsymbol{g}} \boldsymbol{B}_q ds \right] \dot{\boldsymbol{q}} = \boldsymbol{J}(\boldsymbol{q}, X)\dot{\boldsymbol{q}} , \tag{15}$$

which defines the geometric Jacobian $\boldsymbol{J}(\boldsymbol{q}, X) \in \mathbb{R}^{6\times n}$ for a variable-strain soft manipulator. Notice that the geometric Jacobian (15) is a generalization of the PCS one obtained in [25], which can be recovered here by setting a constant strain basis $\boldsymbol{B}_q(X) = \boldsymbol{B}_q$ and recalling that $\int_0^X \mathrm{Ad}_{\boldsymbol{g}} ds = \boldsymbol{T}_g(X)$ is the tangent operator of the exponential map.

B. Discrete Statics

It is now possible to obtain the generalized static equation of the system by virtue of the D'Alembert's principle. Projecting the continuous static model (8) with the transpose of the Jacobian $\boldsymbol{J}^T$ and integrating over the length of the rod [34], we obtain the following sequence of identities (note that $\mathrm{Ad}_{\boldsymbol{g}}^T = \mathrm{Ad}^*_{\boldsymbol{g}^{-1}}$):

$$\begin{aligned}
&\int_0^L \boldsymbol{J}^T \left[\left(\boldsymbol{\mathcal{F}}_i - \boldsymbol{\mathcal{F}}_a\right)' + \mathrm{ad}^*_{\boldsymbol{\xi}} \left(\boldsymbol{\mathcal{F}}_i - \boldsymbol{\mathcal{F}}_a\right) \right] dX = \boldsymbol{0} , \\
&\int_0^L \boldsymbol{J}^T \left[\mathrm{Ad}^*_{\boldsymbol{g}^{-1}} \left(\mathrm{Ad}^*_{\boldsymbol{g}} \left(\boldsymbol{\mathcal{F}}_i - \boldsymbol{\mathcal{F}}_a\right)\right)' \right] dX = \boldsymbol{0} , \\
&\int_0^L \left(\int_0^X \boldsymbol{B}_q^T \mathrm{Ad}^*_{\boldsymbol{g}^{-1}} ds \right) \left(\mathrm{Ad}^*_{\boldsymbol{g}} \left(\boldsymbol{\mathcal{F}}_i - \boldsymbol{\mathcal{F}}_a\right)\right)' dX = \boldsymbol{0} .
\end{aligned}$$

Finally, integrating by part and inserting the boundary condition given in (8) yields to the following generalized static equation:

$$\int_0^L \boldsymbol{B}_q^T \boldsymbol{\mathcal{F}}_i dX = \int_0^L \boldsymbol{B}_q^T \boldsymbol{\mathcal{F}}_a dX . \tag{16}$$

C. Actuation Load Basis

Now, consider a Cosserat rod internally actuated by several tendons and/or fluidic chambers. In the general case, the actuation load (10) can be represented in the form:

$$\boldsymbol{\mathcal{F}}_a(X) = \sum_{i=1}^{n_a} \begin{bmatrix} \tilde{\boldsymbol{d}}_i(X)\boldsymbol{t}_i(X) \\ \boldsymbol{t}_i(X) \end{bmatrix} \tau_i = \boldsymbol{B}_\tau(\boldsymbol{q}, X)\boldsymbol{\tau} , \tag{17}$$

where $\boldsymbol{B}_\tau(\boldsymbol{q}, X) \in \mathbb{R}^{6\times n_a}$ is a matrix function whose columns are given by vector functions as in (10) and $\boldsymbol{\tau} \in \mathbb{R}^{n_a}$ is the vector of magnitude actuation forces. Inserting equations (9), (14) and (17) into the generalized static equation (16), allows to write the static equilibrium in the form:

$$\boldsymbol{K}\boldsymbol{q} = \boldsymbol{B}(\boldsymbol{q})\boldsymbol{\tau} , \tag{18}$$

where

$$\boldsymbol{K} = \int_0^L \boldsymbol{B}_q^T \boldsymbol{\Sigma} \boldsymbol{B}_q dX \in \mathbb{R}^{n\times n} ,$$

is the generalized stiffness matrix and

$$\boldsymbol{B}(\boldsymbol{q}) = \int_0^L \boldsymbol{B}_q^T \boldsymbol{B}_\tau(\boldsymbol{q}) dX \in \mathbb{R}^{n\times n_a} ,$$

is the generalized actuation matrix.

The main benefits of this new generalized static equations (18) are twofold. First, it represents an equivalent but simplified version of the continuous model (12), which is converted into a simple algebraic equation with a finite number of DOFs, potentially small even for complex deformations. It should be noticed that, thanks to the variable-strain basis, an accurate result can be achieved with a much lower number of DOFs with respect to the constant-strain approach. Secondly, equation (18) provides an explicit formula in the standard minimal matrix form, which is particularly suitable for control design. Furthermore, a generalized actuation matrix $\boldsymbol{B}(\boldsymbol{q})$ is provided for the first time. A clever choice of the strain basis, that would not have been possible with the constant-strain approach, leads to the simplest form of the static equilibrium with the minimal number of DOFs. As a matter of fact, taking

$$\boldsymbol{B}_q(\boldsymbol{q}, X) = \boldsymbol{\Sigma}(X)^{-1}\boldsymbol{B}_\tau(\boldsymbol{q}, X) \ , \tag{19}$$

yields to the trivial form

$$\left[\int_0^L \boldsymbol{B}_\tau^T \boldsymbol{\Sigma}^{-1}\boldsymbol{B}_\tau dX\right](\boldsymbol{q} - \boldsymbol{\tau}) = \boldsymbol{0} \rightarrow \boldsymbol{q} = \boldsymbol{\tau} \ , \tag{20}$$

where the number of DOFs is equal to the number of actuators (*i.e.,* $n = n_a$). Note that the matrix on the left of equation (20) is equivalent to $\boldsymbol{K}$, given (19), and symmetric positive-definite if the actuators are linearly independent.

D. Solution Discrete Model

The discrete model (18) is a non-linear algebraic equation that can be numerically solved for $\boldsymbol{q}$. Once the vector $\boldsymbol{q}$ is found, the strain filed $\boldsymbol{\xi}$ is obtained with (14), from which the manipulator's configuration $\boldsymbol{g}(X)$ can be reconstructed using (5). For the special choice of basis (19) the reconstruction equation (14) becomes:

$$\boldsymbol{\xi}(X) = \boldsymbol{\Sigma}(X)^{-1}\boldsymbol{B}_\tau(\boldsymbol{\xi}, X)\boldsymbol{\tau} + \boldsymbol{\xi}^* \ . \tag{21}$$

Remarkably, equation (21) can be solved for $\boldsymbol{\xi}$ for any X independently and in any order effectively decoupling the problem. As in the previous case, the manipulator's configuration $\boldsymbol{g}(X)$ can then be reconstructed using (5). Equation (21) provides a simple, concise and yet accurate interpretation of the relationship between the actuator force and the robot arm deformation, which can be convenient for mechanical and control design.

IV. Application and Comparison

In this section, the continuous model (12), the general discrete model (18) and the trivial form (20) are applied to different cases and compared in term of accuracy and complexity (*i.e.,* number of DOFs). The continuous model (12) is taken as benchmark to validate the accuracy of the variable-strain approach proposed in this letter.

A. Linear Actuator Path

First, we consider the case of linear actuator path, where the actuation load $\boldsymbol{\mathcal{F}}_a(X)$ (10) is completely determined by the distance $\boldsymbol{d}(X)$ between the actuator and the midline, parametrized as:

$$\boldsymbol{d}(X) = \left[0;\ d_y + \bar{d}_y X;\ d_z + \bar{d}_z X\right]^T \ . \tag{22}$$

TABLE I
Actuator Parameters for the Linear Path Cases

	Constant	**Oblique**	**Multiple**		
			Act. 1	Act. 2	Act. 3
d_y [m]	$R_t/2$	$R_t/2$	0	0	$-R_t/2$
$\bar{d}_y$ [-]	0	$-R_t/L$	$R_t/2L$	$R_t/2L$	0
d_z [m]	0	0	$R_t/2$	$-R_t/2$	0
$\bar{d}_z$ [-]	0	0	$-R_t/2L$	$R_t/2L$	0
$\boldsymbol{\tau}$ [N]	[-7.5,7.5]	[-15,15]	[-15,15]	[-15,15]	[-15,15]

TABLE II
Strain Bases for the Linear Path Cases

	Prescribed	n	Strain-dept.	n
Constant	$\begin{bmatrix} 0 & 0 & 1 & 0 & 0 & 0 \\ 0 & 0 & 0 & 1 & 0 & 0 \end{bmatrix}^T$	2	$\boldsymbol{\Sigma}^{-1}\boldsymbol{B}_\tau$	1
Oblique	$\begin{bmatrix} 0 & 0 & 1 & 0 & 0 & 0 \\ 0 & 0 & X & 0 & 0 & 0 \\ 0 & 0 & 0 & 1 & 0 & 0 \end{bmatrix}^T$	3	$\boldsymbol{\Sigma}^{-1}\boldsymbol{B}_\tau$	1
Multiple	$\begin{bmatrix} 1 & 0 & 0 & 0 & 0 & 0 \\ X & 0 & 0 & 0 & 0 & 0 \\ & & \vdots & & & \\ 0 & 0 & 0 & 0 & 0 & 1 \\ 0 & 0 & 0 & 0 & 0 & X \end{bmatrix}^T$	6	$\boldsymbol{\Sigma}^{-1}\boldsymbol{B}_\tau$	2

We consider a circular cross-section robotic arm having a total length of 0.75 m, 0.01 m base R_b and tip R_t radius, $5.93 \cdot 10^5$ Pa Young modulus E and $2.00 \cdot 10^5$ Pa shear modulus G. The actuator parameters used in the simulations are given in Table I. We take into account three cases: (A1) the actuator path is parallel to the robot arm midline (Constant), (A2) the actuator path is coplanar with the robot arm midline (Oblique), and (A3) multiple actuators including out-of-plane paths (Multiple). For each case, a suitable strain basis for the discrete model (18) is chosen based on the distance vector function $\boldsymbol{d}(X)$, with the intent of faithfully represent the deformed configuration with a minimum number of DOFs (Table II). For instance, since the actuators' path is linear (22), we expect to reasonably match the robot arm deformation with at most two DOFs for each strain, one for the constant term and one for the linear term. For what concerns the trivialized model (20), the strain basis is given by (19) which is capable of further reducing the number of DOFs (equal to the number of actuators) and improve the accuracy. The results of the comparison for different magnitude of the actuator forces is given in Fig. 2 (left column). As can be seen there, the deformed configurations for all the three models are indistinguishable in all the cases. This is reflected in the strain comparison, which highlights only minor deviations between the three models. Note that only the torsional strain of case (A3) presents a non-linear trend that is not captured by the prescribed linear basis. This comparison demonstrates the feasibility and the benefits of the proposed approach for the case of linear actuator paths and cylindrical cross-sections.

The case (A2) is also compared with the PCS model, in order to highlight the benefits of the new approach. The results are reported in Fig. 3 for a 3 sections PCS, each with constant basis for the bending and elongation strains (6 DOFs in total). Despite using twice the DOFs of the variable-strain model, the PCS model is clearly not able to accurately match the linearly decreasing bending.

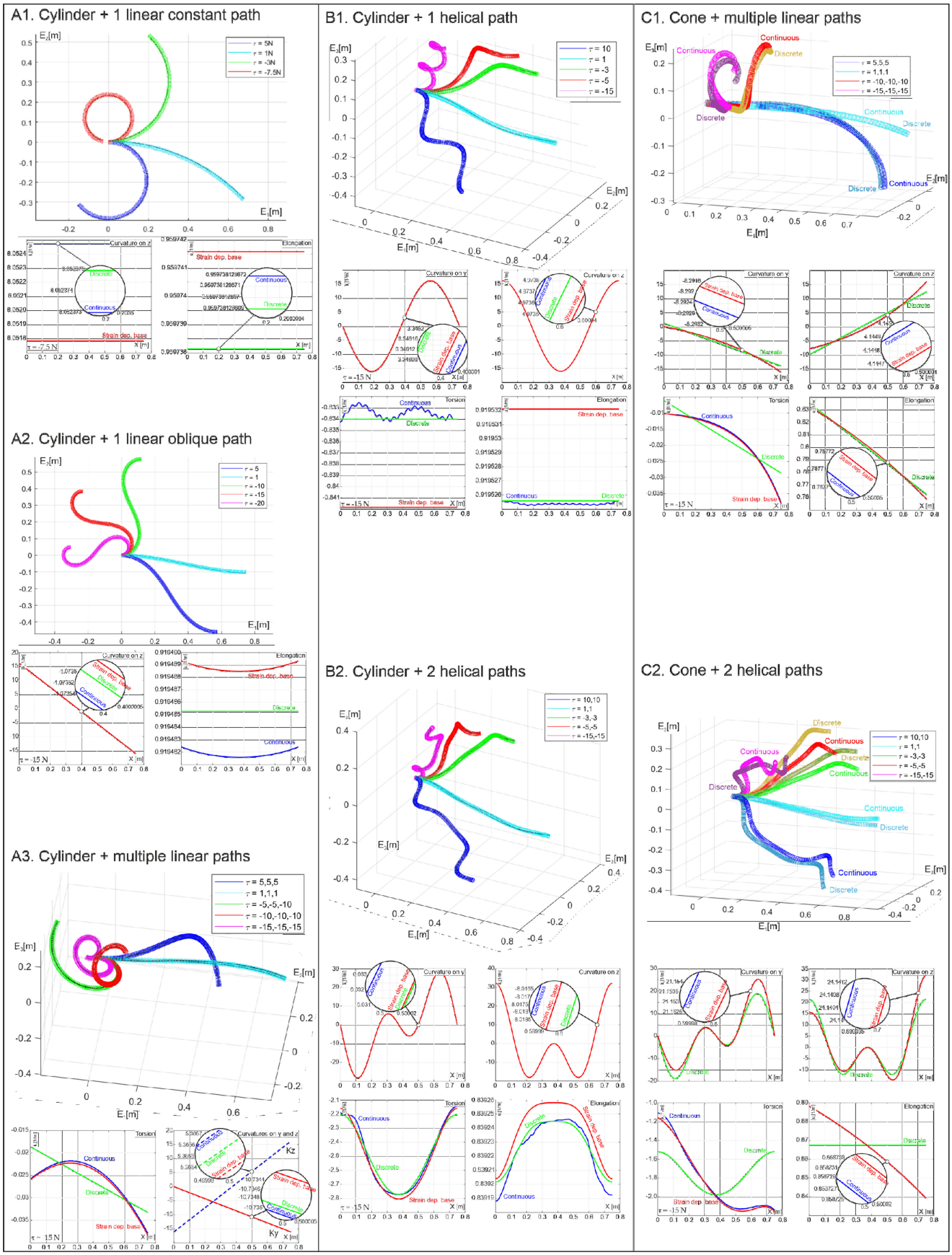

Fig. 2. Comparison between the deformed configurations and the strains obtained for the all the considered geometries and tendon paths. (Left column) Cylindrical arm with linear paths: perpendicular actuator (A1), co-planar actuator (A2) and multiple out-of-plane actuators (A3). (Middle column) Cylindrical arm with (B1) single and (B2) helical paths. (Right column) Conical arm with multiple linear (C1) and helical paths (C2).

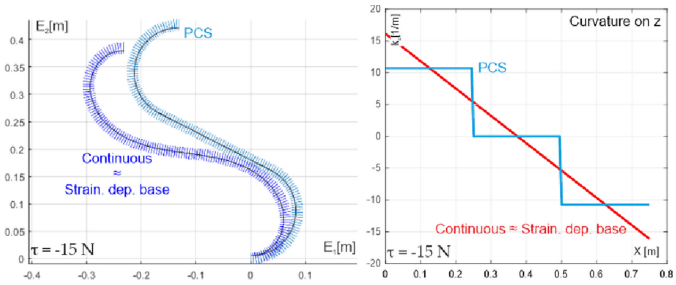

Fig. 3. Comparison between (left) the deformed shapes and (right) the corresponding curvature along the z axis, obtained with the PCS model and the continuous and trivialized ones.

TABLE III
ACTUATOR PARAMETERS FOR THE HELICAL PATH CASES

	Single	**Multiple**	
		Actuator 1	Actuator 2
d [m]	$R_t/2$	$R_t/2$	$R_t/2$
α []	1.529	1.529	1.487
$\boldsymbol{\tau}$ [N]	[-15,15]	[-15,15]	[-15,15]

TABLE IV
STRAIN BASES FOR THE HELICAL CASES ($\omega_* := \frac{2\pi}{p_*}$)

	Prescribed	n	Strain-dept	n
Single	$\begin{matrix}\text{diag}\\(1, \sin(\omega_1 X), \cos(\omega_1 X),\\ 1, \sin(\omega_1 X), \cos(\omega_1 X))\end{matrix}$	6	$\boldsymbol{\Sigma}^{-1}\boldsymbol{B}_\tau$	1
Multiple	$\begin{matrix}\text{blockdiag}\\([1\ \cos(\omega_1 X)\ \cos(\omega_2 X)],\\ [\sin(\omega_1 X)\ \sin(\omega_2 X)],\\ [\cos(\omega_1 X)\ \cos(\omega_2 X)],\\ 1, [\sin(\omega_1 X)\ \sin(\omega_2 X)],\\ [\cos(\omega_1 X)\ \cos(\omega_2 X)])\end{matrix}$	12	$\boldsymbol{\Sigma}^{-1}\boldsymbol{B}_\tau$	2

B. Helical Actuator Path

As second test, we have compared the three models for the case of helical actuator paths, defined by:

$$\boldsymbol{d}(X) = \left[0;\ d\cos\left(\frac{2\pi}{p}X\right);\ d\sin\left(\frac{2\pi}{p}X\right)\right]^T, \qquad (23)$$

where d is the magnitude of the distance between the actuator and the midline and p is the pitch of the helix equal to $p = 2\pi d\tan(\alpha)$, α being the angle enclosed between the actuator path and the arm cross-section. The robotic arm parameters are the same as before, while the actuator parameters are given in Table III. Here, we consider two cases: (B1) single helical actuator and (B2) multiple helical actuators with different pitches. As for the linear path, the basis vector functions for the discrete model are chosen following the distance vector (23), *i.e.,* trigonometric functions with the same frequency rotated by the cross product with $\boldsymbol{t}$ (Table IV).The results of the second test are reported in Fig. 2(middle column). As for the linear paths, the deformed configurations are indistinguishable between the three models. As highlighted by the strain comparison, we note that the small deviation is caused by the torsional strain, whose trend incorporates signals at different frequencies than the ones expressed by the strain basis. This comparison demonstrates the feasibility of the proposed approach for the case of spiral actuator paths and cylindrical cross-sections.

C. Conical Cross-Section

In this last test, we have applied the three models to a conical cross-section manipulator with multiple linear and spiral actuators. In particular, we consider the same manipulator as in the previous tests with a 20% thicker base radius ($R_b = 0.012$ m), while, as per the actuator paths, we use the multiple cases of the linear test (C1) and the helical test (C2) described in Tables I and III respectively. A conical cross-section leads to a non-linear (polynomial) rod elasticity matrix $\boldsymbol{\Sigma}(X)$, which in turn influences the robot arm strains. The mixed contributions of rod elasticity and actuator path geometry are automatically caught by the strain-dependent basis of the trivialized model, while the prescribed basis of the general discrete model needs to be adequately augmented to capture the additional modes due to the varying elastic properties. This would be possible by including a polynomial basis of increasing grade as long as necessary. However, in order to highlight the effect of the non-linear elasticity and the benefits of the strain-dependent parametrization, the bases of the two variable-strain models are kept identical to the cylindrical case, and are described in the last row of Tables II and IV. The results of the comparison are shown in Fig. 2. As expected, the trivialized model matches the continuum model accurately, while the discrete model with the prescribed basis significantly deviates from it. Remarkably though, even for the prescribed case, the discrete model is able to adjust its results and perform a sort of *a priori* curve fitting given the available basis.

V. CONCLUSIONS

A new geometric variable-strain approach has been presented, which extends the constant-strain approach of [24] to the case of non-constant strain, allowing the modelling of complex deformed configurations with a reduced number of DOFs. In the process, a new geometric Jacobian for soft robots has been developed and a generalized actuation matrix has been proposed for the first time. The proposed model have been tested against the PCS approach and a full Cosserat continuous model, for different cross section geometries, actuator paths and force magnitudes. The new discrete model has demonstrated excellent results in all the cases, both in terms of accuracy and complexity (number of DOFs required), especially in its trivialized form. Presented here for the simplified case of single section in static equilibrium, the model yielded to a simple and yet accurate interpretation of the relationship between the actuator force and the robot arm deformation, which can be useful for mechanical and control design. Following the same procedure proposed in [25], the approach will be extended in a future manuscript to the multi-section, floating base, dynamic case, including hybrid soft-rigid bodies.

APPENDIX A
FORMULAS

Adjoint Representations

$$\mathrm{Ad}_{\boldsymbol{g}} = \begin{pmatrix} \boldsymbol{R} & \boldsymbol{0}_{3\times3} \\ \tilde{\mathsf{u}}\boldsymbol{R} & \boldsymbol{R} \end{pmatrix}, \ \mathrm{Ad}^*_{\boldsymbol{g}} = \begin{pmatrix} \boldsymbol{R} & \tilde{\mathsf{u}}\boldsymbol{R} \\ \boldsymbol{0}_{3\times3} & \boldsymbol{R} \end{pmatrix},$$

$$\mathrm{ad}_{\boldsymbol{\xi},\boldsymbol{\eta}} = \begin{pmatrix} \widetilde{\mathsf{k}},\widetilde{\mathsf{w}} & \boldsymbol{0}_{3\times3} \\ \widetilde{\mathsf{u}},\widetilde{\mathsf{v}} & \widetilde{\mathsf{k}},\widetilde{\mathsf{w}} \end{pmatrix}, \quad \mathrm{ad}^*_{\boldsymbol{\xi},\boldsymbol{\eta}} = \begin{pmatrix} \widetilde{\mathsf{k}},\widetilde{\mathsf{w}} & \widetilde{\mathsf{u}},\widetilde{\mathsf{v}} \\ \boldsymbol{0}_{3\times3} & \widetilde{\mathsf{k}},\widetilde{\mathsf{w}} \end{pmatrix}$$

B. Exponential Map

$$\exp\left(\widehat{\boldsymbol{\Omega}}(X)\right) = \boldsymbol{I}_4 + \widehat{\boldsymbol{\Omega}} + \frac{(1-\cos(\theta))}{\theta^2}\widehat{\boldsymbol{\Omega}}^2 + \frac{(\theta-\sin(\theta))}{\theta^3}\widehat{\boldsymbol{\Omega}}^3$$
$$\text{with } \theta = \| [\boldsymbol{\Omega}]_3 \| \tag{24}$$

REFERENCES

[1] C. Laschi, B. Mazzolai, and M. Cianchetti, "Soft robotics: Technologies and systems pushing the boundaries of robot abilities," *Sci. Robot.*, vol. 1, no. 1, 2016, Art. no. eaah3690.

[2] T. G. Thuruthel, Y. Ansari, E. Falotico, and C. Laschi, "Control strategies for soft robotic manipulators: A survey," *Soft Robot.*, vol. 5, no. 2, pp. 149–163, 2018.

[3] R. Kang, D. T. Branson, E. Guglielmino, and D. G. Caldwell, "Dynamic modeling and control of an octopus inspired multiple continuum arm robot," *Comput. Math. Appl.*, vol. 64, no. 5, pp. 1004–1016, 2012.

[4] H. Hossein, C. Yang, I. S Godage, R. Kang, I. D Walker, and D. T Branson III, "A lumped-mass model for large deformation continuum surfaces actuated by continuum robotic arms," *ASME J. Mechanisms Robot.*, vol. 12, 2019, Art. no. 011014.

[5] C. Duriez, "Control of elastic soft robots based on real-time finite element method," in *Proc. IEEE Int. Conf. Robot. Autom.*, May 2013, pp. 3982–3987.

[6] O. Goury and C. Duriez, "Fast, generic, and reliable control and simulation of soft robots using model order reduction," *IEEE Trans. Robot.*, vol. 34, no. 6, pp. 1565–1576, Dec. 2018.

[7] M. Thieffry, A. Kruszewski, C. Duriez, and T. Guerra, "Control design for soft robots based on reduced-order model," *IEEE Robot. Autom. Lett.*, vol. 4, no. 1, pp. 25–32, Jan. 2019.

[8] G. S. Chirikjian, "A continuum approach to hyper-redundant manipulator dynamics," in *Proc. IEEE/RSJ Int. Conf. Intell. Robots Syst.*, Jul. 1993, vol. 2, pp. 1059–1066.

[9] A. Macchelli, C. Melchiorri, and S. Stramigioli, "Port-based modeling and simulation of mechanical systems with rigid and flexible links," *IEEE Trans. Robot.*, vol. 25, no. 5, pp. 1016–1029, Oct. 2009.

[10] I. A. Gravagne, C. D. Rahn, and I. D. Walker, "Large deflection dynamics and control for planar continuum robots," *IEEE/ASME Trans. Mechatronics*, vol. 8, no. 2, pp. 299–307, Jun. 2003.

[11] D. Trivedi, A. Lotfi, and C. D. Rahn, "Geometrically exact dynamic models for soft robotic manipulators," in *Proc. IEEE/RSJ Int. Conf. Intell. Robots Syst.*, Oct 2007, pp. 1497–1502.

[12] D. C. Rucker and R. J. Webster, "Statics and dynamics of continuum robots with general tendon routing and external loading," *IEEE Trans. Robot.*, vol. 27, no. 6, pp. 1033–1044, Dec. 2011.

[13] F. Renda, M. Giorelli, M. Calisti, M. Cianchetti, and C. Laschi, "Dynamic model of a multibending soft robot arm driven by cables," *IEEE Trans. Robot.*, vol. 30, no. 5, pp. 1109–1122, Oct. 2014.

[14] F. Boyer, M. Porez, and W. Khalil, "Macro-continuous computed torque algorithm for a three-dimensional eel-like robot," *IEEE Trans. Robot.*, vol. 22, no. 4, pp. 763–775, Aug. 2006.

[15] J. Till, V. Aloi, and C. Rucker, "Real-time dynamics of soft and continuum robots based on cosserat rod models," *Int. J. Robot. Res.*, vol. 38, no. 6, pp. 723–746, 2019.

[16] M. Giorelli, F. Renda, M. Calisti, A. Arienti, G. Ferri, and C. Laschi, "Neural network and jacobian method for solving the inverse statics of a cable-driven soft arm with nonconstant curvature," *IEEE Trans. Robot.*, vol. 31, no. 4, pp. 823–834, Aug. 2015.

[17] T. G. Thuruthel, E. Falotico, F. Renda, and C. Laschi, "Model-based reinforcement learning for closed-loop dynamic control of soft robotic manipulators," *IEEE Trans. Robot.*, vol. 35, no. 1, pp. 124–134, Feb. 2019.

[18] W. S. Rone and P. Ben-Tzvi, "Continuum robot dynamics utilizing the principle of virtual power," *IEEE Trans. Robot.*, vol. 30, no. 1, pp. 275–287, Feb. 2014.

[19] I. S. Godage, G. A. Medrano-Cerda, D. T. Branson, E. Guglielmino, and D. G. Caldwell, "Dynamics for variable length multisection continuum arms," *Int. J. Robot. Res.*, vol. 35, no. 6, pp. 695–722, 2015.

[20] V. Falkenhahn, A. Hildebrandt, R. Neumann, and O. Sawodny, "Dynamic control of the bionic handling assistant," *IEEE/ASME Trans. Mechatronics*, vol. 22, no. 1, pp. 6–17, Feb. 2017.

[21] K. M. Lynch and F. C. Park, *Modern Robotics: Mechanics, Planning, and Control*. Cambridge, U.K.: Cambridge Univ. Press, 2017.

[22] A. De Luca, "Dynamic control of robots with joint elasticity," in *Proc. IEEE Int. Conf. Robot. Autom.*, Apr. 1988, vol. 1, pp. 152–158.

[23] C. Della Santina, R. K. Katzschmann, A. Biechi, and D. Rus, "Dynamic control of soft robots interacting with the environment," in *Proc. IEEE Int. Conf. Soft Robot. (RoboSoft)*, Apr. 2018, pp. 46–53.

[24] F. Renda, F. Boyer, J. Dias, and L. Seneviratne, "Discrete cosserat approach for multisection soft manipulator dynamics," *IEEE Trans. Robot.*, vol. 34, no. 6, pp. 1518–1533, Dec. 2018.

[25] F. Renda and L. Seneviratne, "A geometric and unified approach for modeling soft-rigid multi-body systems with lumped and distributed degrees of freedom," in *Proc. IEEE Int. Conf. Robot. Autom.*, May 2018, pp. 1567–1574.

[26] J. C. Simo, "A finite strain beam formulation. the three-dimensional dynamic problem, part i," *Comput. Methods Appl. Mechanics Eng.*, vol. 49, no. 1, pp. 55–70, 1985.

[27] F. Boyer and D. Primault, "Finite element of slender beams in finite transformations: a geometrically exact approach," *Int. J. Numer. Methods Eng.*, vol. 59, no. 5, pp. 669–702, 2004.

[28] V. Sonneville, A. Cardona, and O. Brüls, "Geometrically exact beam finite element formulated on the special Euclidean group SE(3)," *Comput. Methods Appl. Mechanics Eng.*, vol. 268, pp. 451–474, 2014.

[29] J. Linn, "Discrete cosserat rod kinematics constructed on the basis of the difference geometry of framed curves–part i: Discrete cosserat curves on a staggered grid, *J. Elasticity*, vol. 139, pp. 177–236, 2020.

[30] P. Cesarek, M. Saje, and D. Zupan, "Dynamics of flexible beams: Finite-element formulation based on interpolation of strain measures," *Finite Elements Anal. Des.*, vol. 72, pp. 47–63, 2013.

[31] R. M. Murray, Z. Li, and S. S. Sastry, *A Mathematical Introduction to Robotic Manipulation*. Boca Raton, FL, USA: Taylor & Francis, 1994.

[32] E. Hairer, C. Lubich, and G. Wanner, *Geometric Numerical Integration: Structure-Preserving Algorithms for Ordinary Differential Equations* (Springer Series in Computational Mathematics). Berlin, Germany: Springer, 2006.

[33] J. M. Selig., *Geometric Fundamentals of Robotics* (Monographs in Computer Science Series). Berlin, Germany: Springer, 2007.

[34] F. Renda, V. Cacucciolo, J. Dias, and L. Seneviratne, "Discrete cosserat approach for soft robot dynamics: A new piece-wise constant strain model with torsion and shears," in *Proc. IEEE/RSJ Int. Conf. Intell. Robots Syst.*, Oct. 2016, pp. 5495–5502.

[35] A. Zanna, "Collocation and relaxed collocation for the FER and the magnus expansions," *SIAM J. Numer. Anal.*, vol. 36, no. 4, pp. 1145–1182, Apr. 1999.

[36] F. Renda, M. Cianchetti, M. Giorelli, A. Arienti, and C. Laschi, "A 3D steady-state model of a tendon-driven continuum soft manipulator inspired by the octopus arm," *Bioinspiration Biomimetics*, vol. 7, no. 2, 2012, Art. no. 025006.

[37] F. Renda, M. Cianchetti, H. Abidi, J. Dias, and L. Seneviratne, "Screw-based modeling of soft manipulators with tendon and fluidic actuation," *J. Mechanism Robot.*, vol. 9, 2017, Art. no. 041012.